

Classification of Hand Movements from EEG using a Deep Attention-based LSTM Network

Guangyi Zhang, *Student Member, IEEE* Vandad Davoodnia, *Student Member, IEEE*, Alireza Sepas-Moghaddam, *Student Member, IEEE*, Yaoxue Zhang, *Senior Member, IEEE*, and Ali Etemad, *Member, IEEE*

Abstract—Classifying limb movements using brain activity is an important task in Brain-computer Interfaces (BCI) that has been successfully used in multiple application domains, ranging from human-computer interaction to medical and biomedical applications. This paper proposes a novel solution for classification of left/right hand movement by exploiting a Long Short-Term Memory (LSTM) network with attention mechanism to learn from sequential data available in the electroencephalogram (EEG) signals. In this context, a wide range of time and frequency domain features are first extracted from the EEG signal and are then evaluated using a Random Forest (RF) to select the most important features. The selected features are arranged as a spatio-temporal sequence to feed the LSTM network, learning from the sequential data to perform the classification task. We conduct extensive experiments with the EEG motor movement/imagery database and show that our proposed solution achieves effective results outperforming baseline methods and the state-of-the-art in both intra-subject and cross-subject evaluation schemes. Moreover, we utilize the proposed framework to analyze the information as received by the sensors and monitor the activated regions of the brain by tracking EEG topography throughout the experiments.

Index Terms—Brain-Computer Interfaces, Electroencephalogram, Deep Learning, Long Short-Term Memory, Attention Mechanism.

I. INTRODUCTION

Electroencephalogram (EEG) records electrical signals from the brain, thus providing the ability to extract valuable information regarding brain activity. EEG-based Brain-Computer Interfaces (BCI) have been widely used in medical and biomedical applications such as analyzing walking and sleeping patterns [1], diagnosing brain tumors [2], and rehabilitation of central nervous system disorders [3]. BCI can also help communicate brain commands and enable the control of artificial limbs [4], especially for people suffering from amyotrophic lateral sclerosis brainstem stroke, brain or spinal injury, cerebral palsy, muscular dystrophies, and other diseases impairing the control and feedback system between brain and muscles.

In recent years, EEG-based movement analysis and classification has been widely used in various applications, ranging from clinical applications to brain-machine interface and robotics. For example, stroke patients are often asked to make

several body movements in response to various visual or electrical stimuli, which allows researchers to monitor the progress of the recovery of the patient's brain injury by analyzing EEG signals [5]. Additionally, such technologies allow for patients with disabilities to control movements of artificial limbs or exoskeletons. In particular, the control of hand movements is of critical importance for patients in order to perform everyday tasks [6].

To tackle the problem of BCI for hand-movement control, a number of solutions have been proposed in the literature [7]–[12]. Generally, two approaches can be used for development of automated methods for BCI, including hand-movement classification from EEG. In the first approach, the system is trained (calibrated) on the intended user and then used for BCI applications (intra-subject). While this approach is effective, it does not result in a generalized off-the-shelf solution for a population of patients. The second approach is to develop a generalized solution that performs across subjects once trained with a dataset (cross-subject). While these approaches are more desired and convenient, they tend to show lower accuracies, which are typically below the standards required to employ such systems in real products and solutions.

In this paper, a deep learning solution for Left/Right (L/R) hand movement classification using an LSTM network with attention mechanism is proposed. Our proposed method includes three main steps: *i*) data pre-processing is performed to reduce the negative effects of signal artifacts, including cross-talk, noise, and power-line interference; *ii*) time and frequency domain features are extracted from EEG, to be then used as inputs to the LSTM input layer; and *iii*) an attention-based LSTM network is designed to learn from the sequential EEG features, and then classify them into distinct L/R movements. The architecture of our proposed solution exploits both long and short-term dependencies within the feature manifold. We utilize both intra-subject and cross-subject evaluation schemes to demonstrate the robustness of our method.

Our contributions are as follows: *i*) The proposed deep model, which has been trained over all the available data (103 subjects) using a 10-fold cross-subject validation scheme, significantly outperforms the state-of-the-art solutions for hand movement classification. *ii*) In order to compare our work to previous studies utilizing the same dataset, we also perform intra-subject classification (using the same network) for each of the 103 subjects separately, and achieve very high accuracies, outperforming previous studies. *iii*) Lastly, we perform a detailed analysis of brain activity through the different stages of stimuli perception and hand movement, and demonstrate

G. Zhang, V. Davoodnia, A. Sepas-Moghaddam and A. Etemad are with the Department of Electrical and Computer Engineering, Queen's University, Kingston, ON, Canada (e-mail: guangyi.zhang@queensu.ca, vandad.davoodnia@queensu.ca, alireza.sepas-moghaddam@queensu.ca, ali.etemad@queensu.ca).

Y. Zhang is with the Department of Computer Science and Technology, Tsinghua University, Beijing, China. (e-mail: zyx@mail.tsinghua.edu.cn).

that our choice of extracted features are in correspondence with the known and expected neurological function of the brain.

II. RELATED WORK

Several classical machine learning methods such as Support Vector Machine (SVM) [13], Linear Discriminant Analysis (LDA), [14], Logistic Regression [15], Quadratic Discriminant Analysis (QDA) [14], k-Nearest Neighbor (kNN) [16], and Naïve Bayes (NB) [16] have been used for classification of movement from EEG signals. However, such approaches often cannot model the nonlinearities observed in high-dimensional multi-channel EEG and feature-sets extracted from them. This especially becomes an issue when attempting to model cross-subject relationships within the dataset.

In addition to classical machine learning methods, deep learning solutions have also been utilized for movement classification from EEG. In [17], [18], a Convolutional Neural Network (CNN) was used to perform classification for left and right motor imaginary movements. Long Short Term Memory (LSTM) networks [19], a type of Recurrent Neural Network (RNN), have recently been proven to be efficient in EEG-based applications. An example of such applications is the prediction of epileptic seizures using EEG signals [20], showing higher performance than other machine learning techniques including SVM, LDA, and CNN. Another example is EEG-based intention recognition studied in [21], in which a very high accuracy was achieved using a parallel or cascade combination of CNN and LSTM networks. Moreover, an LSTM-based model was proposed in [22] for EEG-based classification of imaginary tasks, outperforming the state-of-the-art solutions including methods based on other deep networks.

In most of the above-mentioned solutions, *intra-subject* classification has been performed, where one classifier is separately trained and tested for each subject, and the average accuracy for all the classifiers is reported. Employing this approach often stems from the fact that distinguishing between L/R hand movements can be a challenging task due to the highly subject-dependant nature of brain activities in the visual and motor cortex. For instance, in [13], an average accuracy of 64.02% was reported using a Common Spatial Patterns (cSPS) approach for 10 subjects in an intra-subject approach. In [14], an average accuracy of 88.69% was reported using QDA, while a rough set-based classifier was used in [23] and [24], reporting average accuracies of 60% and 68% respectively.

EEG-based movement classification can be very challenging with a *cross-subject* scheme, where a single model needs to be trained for the entire dataset and generalize to all the subjects. The results presented in [25] showed that the average accuracy dropped from 87% to chance level (50%), when utilizing a cross-subject scheme instead of an intra-subject one, using the proposed Maximum Discernibility Algorithm (MDA). Another cross-subject classification solution was proposed in [26], where a selected set of time and frequency domain features was fed to an Artificial Neural Network (ANN), achieving an accuracy of 68%. Moreover, a large-scale synchronization analysis using Phase Locking Value (PLV) was provided in

[27], defining a criteria that could successfully distinguish between L/R hand movement and obtain an average accuracy of 78.95%.

As observed by the studies above, a number of solutions have been proposed for movement recognition from EEG. However, our study of the literature suggests that when cross-subject schemes are used, the performance of the proposed methods are not robust enough to allow for practical applications of such technologies. We tackle this problem in our work and propose a robust solution capable of outperforming the state-of-the-art by a considerable margin.

III. PROPOSED METHOD

This section presents the proposed method, exploiting an LSTM network with attention mechanism to learn from preprocessed and pre-selected time and frequency features available in the EEG signals.

A. Pre-processing

Data pre-processing was performed to reduce the negative effects of signal artifacts, including cross-talk, noise, and power-line interference. In this context, out of the 64 EEG channels available in the EEG test material, the 10 central sensors were discarded due to their non-symmetric nature [28]. The utilized sensor pairs were selected based on the topology described in [28]. Then, two filters were applied to the new 27 differential EEG channels: a notch filter removed 50 Hz power line interference and a band-pass filter was applied to allow a frequency range of 0.5 – 70 Hz to pass through, thus minimizing artifacts such as noise often present in this frequency range [29]. Normalization of EEG amplitude was then carried out as the last step to minimize the difference in EEG amplitudes across different subjects. If $x = [x_1, x_2, \dots, x_N]$ represents a particular segment of the signal, the applied min-max normalization is described as $x_{norm} = 2 \times [x - \min(x)] / [\max(x) - \min(x)] - 1$.

B. Time and Frequency Domain Feature Extraction

Successive to pre-processing, a number of time and frequency domain features were extracted in order to be used as inputs for the proposed method. EEG is known as a non-stationary time-series signal where nonlinear features are often used for representation and classification tasks. Feature extraction was performed on a 2-second segment of each trial. The segmentation window size was selected empirically for maximizing performance. Time and frequency domain features were subsequently extracted from each time-step. Time-domain features included: *i*) mean, *ii*) variance, *iii*) skewness, *iv*) kurtosis, *v*) zero crossings, *vi*) absolute area under the signal, and *vii*) peak-to-peak distance. Extracted frequency-domain features consisted of relative band power in four frequency bands, notably *i*) delta (0.5 – 4 Hz), *ii*) theta (4 – 8 Hz), *iii*) alpha (8 – 12 Hz), and *iv*) beta (12 – 30 Hz). Table I presents the mathematical equations for these features, where a total of 297 features (27 channels \times 11 features per channel) were extracted from each time-step.

TABLE I
TIME AND FREQUENCY DOMAIN FEATURES

Method	Formula
Mean	$\mu = \frac{1}{N} \sum_{i=1}^N x_i$
Variance	$\sigma^2 = \frac{1}{N} \sum_{i=1}^N (x_i - \mu)^2$
Skewness	$S = \frac{\frac{1}{N} \sum_{i=1}^N (x_i - \mu)^3}{(\frac{1}{N-1} \sum_{i=1}^N (x_i - \mu)^2)^{3/2}}$
Kurtosis	$K = \frac{\frac{1}{N} \sum_{i=1}^N (x_i - \mu)^4}{(\frac{1}{N} \sum_{i=1}^N (x_i - \mu)^2)^2} - 3$
Zero-crossing	$zc = \sum_{i=1}^{N-1} 1_{\mathbb{R}_{<0}}(x_i x_{i-1})$
Absolute area under signal	$simps = \int_a^b f(x) dx$
Peak to Peak	$pk2pk = \max(X) - \min(X)$
Amplitude spectrum density	$\hat{X}(\omega) = \frac{1}{\sqrt{T}} \int_0^T x(t) \exp^{-i\omega t} dt$
Power spectrum density	$S_{xx}(\omega) = \lim_{T \rightarrow \infty} E \left[\hat{X}(\omega) ^2 \right]$
power of each frequency band	$P = \frac{1}{\pi} \int_{\omega_1}^{\omega_2} S_{xx}(\omega) d\omega$

C. Feature Selection

Feature selection is widely used in EEG studies to reduce the dimensionality of the extracted features, and ultimately aid in better representation and generalization through the use of simpler classifiers [30]. In this paper, we used Random Forest (RF) in order to evaluate the importance of each feature and select the ones with the highest importance scores [31]. The top-30 subject-independent features were selected and utilized for analysis.

D. Motion Description and Classification Model

To detect and classify very subtle spatio-temporal (EEG amplitude or feature values vs. time) changes in our feature space that correspond to the intended movements, a solution capable of remembering and eventually *aggregating* these transitions across the dataset is required. Addressing both these requirements formed the intuition behind our proposed solution of using an LSTM network with the *attention* mechanism. This proposed solution possesses the properties required for describing spatio-temporal properties and aggregate them to produce a final decision. Furthermore, attention-based LSTM has been used in other tasks requiring remembering and aggregation of feature embeddings, notably natural language processing (NLP) [32], [33]. In the following subsection we describe the architecture of a general LSTM cell as well as the attention mechanism.

1) *LSTM Network*: RNNs can be used to extract higher dimensional dependencies from sequential data such as EEG time-series [34]. RNN units have connections not only between the subsequent layers, but also among themselves to

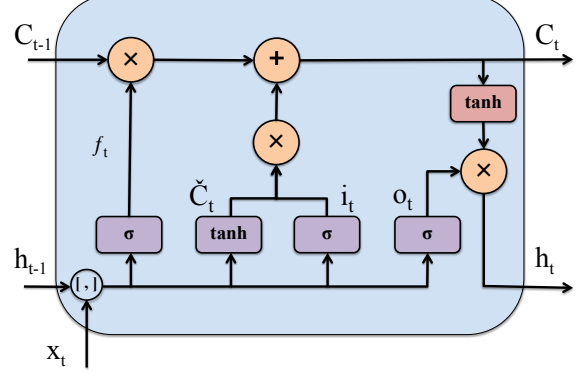


Fig. 1. LSTM Cell Architecture. $[\cdot]$ denotes array concatenation.

capture information from previous inputs. Traditional RNNs can easily learn short-term dependencies; however, they have difficulties in learning long-term dynamics due to the vanishing and exploding gradient problems [35]. LSTM is a type of RNN addressing the vanishing and exploding gradient problems by learning both long- and short-term dependencies [36].

An LSTM network is composed of cells, whose outputs evolve through the network based on past memory content. The cells have a common cell state, which keeps long-term dependencies along the entire LSTM chain of cells. The flow of information is then controlled by the input gate (i_t) and forget gate (f_t), thus allowing the network to decide whether to forget the previous state (C_{t-1}) or update the current state (C_t) given new information. The output of each cell, a hidden state, is controlled by an output gate (o_t), allowing the cell to compute its output given the updated cell state as shown in Figure 1.

The formulas describing an LSTM cell architecture are presented as:

$$i_t = \sigma(W_i \cdot [h_{t-1}, x_t] + b_i), \quad (1)$$

$$f_t = \sigma(W_f \cdot [h_{t-1}, x_t] + b_f), \quad (2)$$

$$C_t = f_t * C_{t-1} + i_t * \tanh(W_c [h_{t-1}, x_t] + b_c), \quad (3)$$

$$o_t = \sigma(W_o \cdot [h_{t-1}, x_t] + b_o), \quad (4)$$

$$h_t = o_t * \tanh(C_t), \quad (5)$$

where h_{t-1} and h_t are the hidden state of the previous and current cells, x_t is the input features fed to the cell, W_f, W_i, W_c, W_o are the weights, and b_f, b_i, b_c, b_o are the biases that can be obtained by backpropagation through time.

2) *Attention Mechanism*: Attention-based LSTM networks have recently been used in many state-of-the-art speech recognition and NLP solutions [32], [37]–[39]. Unlike conventional LSTM networks that use their last hidden state as output, an LSTM network with attention mechanism multiplies the output hidden states by trainable weights, as shown in Figure 2, thus

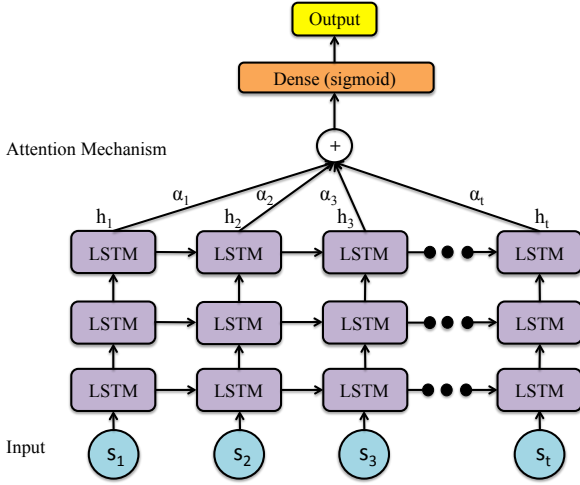


Fig. 2. An overview of LSTM network with attention mechanism.

capturing more discriminative task-related features. This can be formulated as:

$$h_i = LSTM(s_i), i \in [1, L], \quad (6)$$

where, h_i is the output hidden state vector for the i^{th} LSTM cell corresponding to the i^{th} input, and L is the number of cells in each recurrent layer of the LSTM network. To capture the importance of each hidden state, attention mechanism is defined as follows:

$$u_i = \tanh(W_s h_i + b_s), \quad (7)$$

$$\alpha_i = \frac{\exp(u_i)}{\sum_j \exp(u_j)}, \quad (8)$$

$$v = \sum_i \alpha_i h_i, \quad (9)$$

where vector v is the attention layer's output, and W_s and b_s are trainable parameters.

3) *Proposed Network*: The features from the 7 time-steps in each segment (as described earlier), were fed to 7 individual cells of the first LSTM layer. We employed three stacked 7-cell layers in our network. The final LSTM layer was followed by an attention layer, which was in turn followed by a dense layer with a sigmoid activation function to predict the probability of each class. The architecture is depicted in Figure 2.

IV. EXPERIMENT SETTINGS

This section presents the test material, optimal LSTM hyper-parameter setting, evaluation protocols, and the state-of-the-art recognition solutions considered for benchmarking purposes.

A. Dataset

The EEG Motor Movement/Imagery Dataset^{1,2} [40], [41] was used in this study. The dataset includes 109 subjects and has been collected using a BCI 2000 system. Participants were

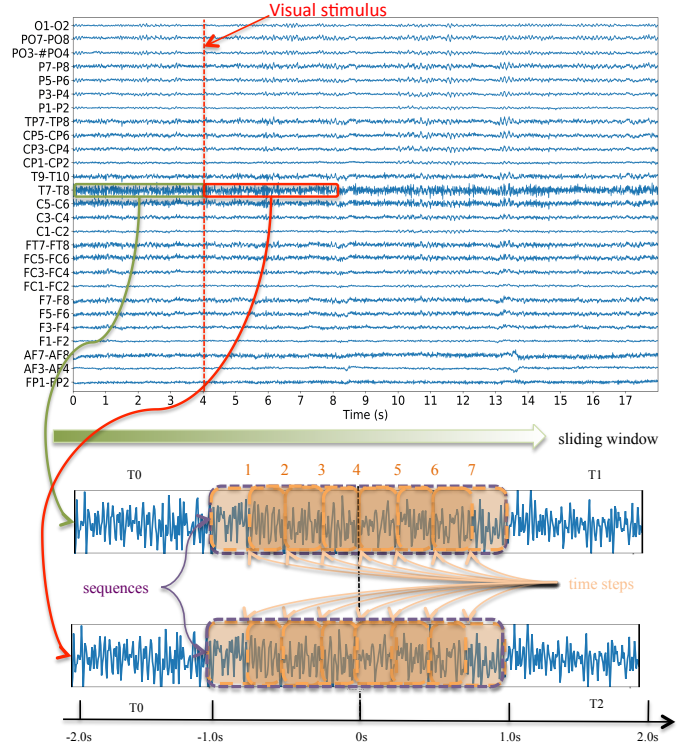


Fig. 3. An overview of the EEG data, the movement segments (2s-long LSTM sequence consists of 7 time steps with 50% overlap between adjacent windows), and the sliding window used during training/classification is illustrated.

asked to perform three actions: rest (T_0), left fist movement (T_1), and right fist movement (T_2). Each experiment consisted of 15 iterations, where T_0 was followed by a visual stimulus, randomly selecting either T_1 or T_2 . This 15-pair movement process was repeated 3 times. Accordingly, the dataset contains a total of $103 \text{ subjects} \times 3 \text{ experiments} \times 15 \text{ movements}$, for a total of 4635 movements. The dataset contains 64-channels of EEG, recorded at a sampling frequency of 160 Hz. Figure 3 illustrates a sample EEG recording and the three actions T_0 , T_1 , and T_2 .

Out of the 109 subjects in the dataset, the data from 6 particular subjects (43, 88, 89, 92, 100, and 104) had low signal to noise ratio. Therefore, they were removed from our dataset. Similar rejection of poor-quality samples has been performed in the literature for the same dataset [14], [23]–[25], [27].

B. LSTM Hyper-Parameters Setting

A number of hyper-parameters for the network were explored and tuned to achieve the best results for our proposed model. Notably, these hyper-parameters include: recurrent depth, batch size, number of training epochs, LSTM hidden layer size, dropout rates applied after input layer and the following three stacked LSTM layers (D_0, D_1, D_2, D_3), and the weight matrix L_2 regularization coefficient of each LSTM layer [42]. Additionally, some hyper-parameters were tuned for the stochastic Adam optimizer [43], such as learning rate (l_r) and exponential decay rates for the first and second

¹<https://physionet.org/pn4/eeegmmidb/>

²www.bci2000.org

TABLE II
TRAINING HYPER-PARAMETERS

Hyperparameters	Cross-Subject	Intra-Subject
Recurrent depth	3	3
Batch size	32	2
Number of training epochs	100	10
LSTM hidden layer size	256	256
Dropout rates	$D0 = 0.0$	$D0 = 0.7$
	$D1 = 0.2$	$D1 = 0.2$
	$D2 = 0.1$	$D2 = 0.1$
	$D3 = 0.2$	$D3 = 0.1$
Learning	$L2 = 0.001, l_r = 0.001$	
	$\beta_1 = 0.9, \beta_2 = 0.999$	

movement estimates (β_1 and β_2). The optimum values for these parameters are presented in Table II. A different set of parameters was assigned for each validation scheme (cross-subject and intra-subject) to maximize performance. A binary cross-entropy loss function $L = -y \log(p) + (1 - y) \log(1 - p)$ was employed for training.

C. Benchmarking

To rigorously evaluate the performance for our proposed solution, we utilized both intra-subject and cross-subject validation schemes. Both schemes used 10-fold cross-validation. We ensured that the split allowed no overlap between the testing and training data, as previous studies with such overlaps have shown to yield very high accuracies as expected [21]. True Positive (TP), False Negative (FN), False Positive (FP), and True Negative (TN) were used to calculate the performance metrics, namely Precision, Recall, and Accuracy, which are formulated as follows:

$$Precision = \frac{TP}{TP + FP}, \quad (10)$$

$$Recall = \frac{TP}{TP + FN}, \quad (11)$$

$$Accuracy = \frac{TP + TN}{TP + TN + FP + FN}. \quad (12)$$

1) *Solutions for Cross-Subject Scheme:* Solutions from related works include: PLV [27] and ANN [26], which have been discussed in Section II. As studies performing cross-subject evaluation on this challenging dataset were not very common, we implemented a number of other classifiers to compare against our proposed method. First, we considered conventional machine learning benchmarking methods such as SVM [16], Naïve Bayes [16], decision tree [44], logistic regression [15], and random forest [45]. The SVM used an 8th degree polynomial kernel and the random forest used 30 estimators up to a depth of 2. These parameters were tuned empirically in order to achieve the best results. The benchmarking solutions included deep learning methods as well. First, we used a 3-layer 2D-CNN, accepting a 2D matrix of 297 features as inputs. The network had a kernel size of 3×3 , and feature maps of 32, 64, and 128, respectively for the first, second, and third convolutional layers. A VGG-16 CNN

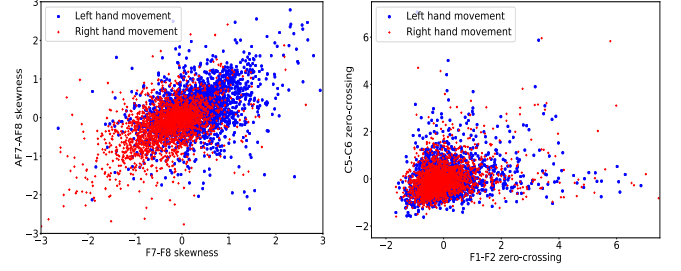


Fig. 4. 2D Scatter plots of the top two and last two selected features using random forest.

was also used for benchmarking. This model was pre-trained on ImageNet [46] and fine-tuned for our application. This model was presented with inputs in the form of 3D matrices, which were achieved by re-sizing the feature matrices to $180 \times 150 \times 1$ using linear interpolation. The output of the VGG-16 convolution layers was followed by 2 dense layers that used ReLu activation and a final output layer with sigmoid activation for estimating the class probabilities. Lastly, an LSTM network without the attention mechanism was also used for benchmarking. In this model, similar hyperparameters as our proposed attention-based method were used (see Table II).

2) *Solutions for Intra-Subject Scheme:* As discussed earlier, the main goal for this work is to tackle the more challenging task of cross-subject generalization. However, to further test our method and compare to the state-of-the-art, we compared our proposed method with solutions from previous studies namely cCSP [13], QDA [14], rough set-based [23], [24], and MDA [25] described in Section II. We did not attempt to utilize more benchmarking solutions in this scheme, as most of the related works in this area utilize intra-subject validation, thus comparing to those works was deemed sufficient.

V. RESULTS AND DISCUSSION

This section reports the experiments conducted for performance assessment. First, we perform feature analysis and then demonstrate the performance of our proposed method along with comparisons to other machine learning techniques and previous studies. Finally, we discuss the most dominant sensors when maximum accuracy is achieved using our method, followed by an analysis of the flow of information during the experiments.

Analysis of Features: As discussed earlier, feature selection was performed using a random forest classifier. The distribution of the top two and last two selected features, based on the ranking of the extracted features, is illustrated in Figure 4. This figure illustrates that the top two selected features, when maximum accuracy is achieved, are almost distributed in two different clusters, while the last two features selected using the random forest method are highly overlapping, thus not very discriminative and valuable for the task at hand.

Evaluation and Comparison: Table III shows the average accuracy, precision, and recall along with their standard deviations within the optimum window for the proposed method

TABLE III
COMPARISON OF DIFFERENT SOLUTIONS USING CROSS-SUBJECT
CLASSIFICATION.

Methods	Accuracy \pm SD	Precision \pm SD	Recall \pm SD
PLV [27]	78.9	—	—
ANN [26]	68.0	—	—
SVM	62.4 \pm 2.1	61.5 \pm 1.7	62.4 \pm 2.1
Logistic Regression	52.9 \pm 1.4	52.4 \pm 2.1	51.1 \pm 1.3
Decision Tree	51.0 \pm 1.3	50.3 \pm 1.3	50.3 \pm 1.3
Random Forest	53.0 \pm 1.2	52.9 \pm 1.6	61.5 \pm 1.4
Naive Bayes	51.1 \pm 1.3	50.7 \pm 1.2	51.2 \pm 1.9
3-layer 2D-CNN	63.2 \pm 1.3	63.1 \pm 1.5	63.1 \pm 1.2
VGG-16	53.2 \pm 1.3	53.1 \pm 2.1	53.2 \pm 1.3
LSTM	77.2 \pm 2.5	77.2 \pm 1.5	76.9 \pm 1.1
LSTM + Attention	83.2 \pm 1.2	83.7 \pm 1.2	82.2 \pm 2.1

TABLE IV
COMPARISON WITH DIFFERENT SOLUTIONS USING INTRA-SUB
CLASSIFICATION.

Method	Accuracy \pm SD	Precision \pm SD	Recall \pm SD
cCSP [13]	64.0	—	—
QDA [14]	88.6	—	—
Rough set [23]	60.0	—	—
Rough set [24]	68.0	—	—
MDA [25]	87.0	—	—
LSTM + Attention	98.3 \pm 0.9	94.7 \pm 1.1	95.9 \pm 1.7

and other benchmarking solutions in the cross-subject scheme setting. These results demonstrate the robust performance of our proposed model compared to other methods. The results show that our proposed model significantly outperforms the best performing benchmarking solution, i.e., PLV, by a considerable 5% accuracy improvement. Additionally, Table IV reports the accuracy, precision, and recall rates obtained for the intra-subject scheme, showing near-perfect performance, while the previous work with the best performance achieved an accuracy of 88.6% [14].

The Receiver Operating Characteristic (ROC) curve, which shows the changes of the TP rate with respect to the FP rate, for the proposed model and the top three benchmarking solutions (in the cross-subject scheme) is illustrated in Figure 5. This figure also includes the Area Under the Curve (AUC) values that reveal the superiority of our proposed approach over the top three benchmarks with an AUC of 0.908.

Discussion: Here we explore the flow of information relevant to L/R hand movement through the sensors over time. The image in Table V shows the sensor distribution based on the international 10-10 system [47], [48]. The table presents the ranking of the sensor pairs based on the number of features selected using the feature extraction and selection method when the highest accuracy is achieved with our proposed solution. It can be observed that the FT7-FT8 sensor pair in the frontal-temporal lobe is the most dominant with 5 features, followed by the T9-T10 sensor pair in the temporal lobe with 4 features. The F7-F8 and T7-T8 sensor pairs, in the frontal and temporal lobes respectively, both have 3 selected features, followed by F5-F6 with 2, and the remaining sensor pairs with 1 or 0 features.

Next we analyze the flow of information at different times during the experiment. In Figure 6, the accuracy of the

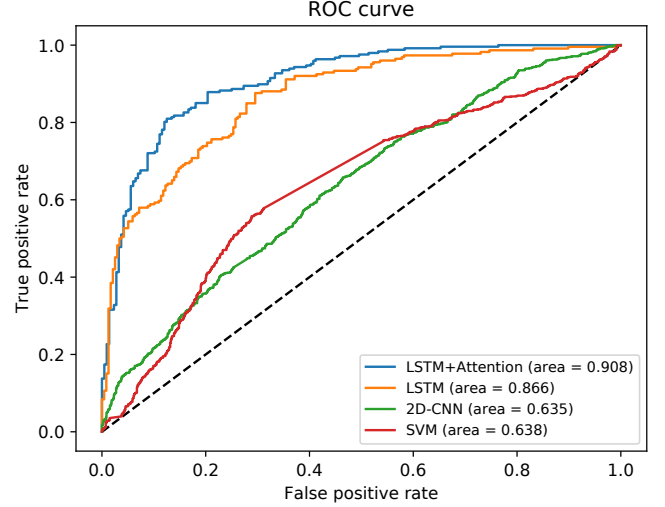
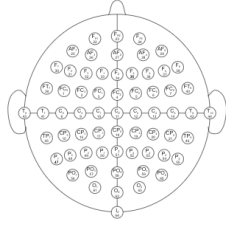


Fig. 5. The ROC curves and corresponding AUCs are presented for our proposed LSTM network and the top-3 benchmarking solutions.

proposed method is depicted along with the standard deviation. The experiment started at $t = 0s$ with the visual stimulus being presented to the subjects. As shown in the figure, in this stage, sensor pairs in the anterior-frontal (AF3-AF4 and AF7-AF8), parietal-occipital (PO3-PO4 and PO7-PO8), and occipital (O1-O2) lobes displayed the strongest features. This phenomenon was consistent with previous studies reporting that the visual cortex plays an important role in receiving and processing visual stimuli [49], [50]. The visual cortex occupies approximately 20% space of the cerebral-cortex and is located in the occipital, parietal-posterior, and temporal lobes [51]. Moreover, the information flow in the parietal-occipital and occipital regions were also consistent with the activities reported in [51], [52].

The $P300$ wave is a type of Event-Related Potential (ERP) that is believed to be dominant in decision-making [53], and is usually within the range of 250ms to 500ms of the onset of visual stimulus [54]. Similar to the $P300$ wave, Simple Reaction Time (SRT) represents the delay between visual stimulus and response, during which the usage of the sensor pairs at $t = 0.25s$ and $t = 0.50s$ shows brain activity. This is consistent with [55], reporting an average and standard deviation of $231 \pm 27ms$ for SRT. During SRT, the previous highly informative sensor pairs in the parietal-occipital and occipital lobes gradually disappeared, and at $t = 0.25s$ sensor pairs in the frontal-temporal (FT7-FT8) and temporal-parietal (TP7-TP8) lobes became more prevalent. The phenomenon was consistent with previous studies, stating that after the receipt of visual stimulus in the visual cortex, visual information is transferred through two disparate streams, notably ventral stream and dorsal stream. Ventral stream eventually reaches the temporal cortex, commonly known for image recognition [56]. The visual stimulus is therefore processed to make the association between experiment instructions and performing L/R hand movement with the help of the relevant memory.

TABLE V
SCALP SENSORS DISTRIBUTED BASED ON THE INTERNATIONAL 10-10 SYSTEM; TOP-30 SUBJECT-INDEPENDENT
FEATURE SELECTION RESULT BASED ON IMPORTANCE WEIGHTS USING RANDOM FOREST.



Rank	Sensor pair	Occurrence	Brain Lobe	Rank	Sensor pair	Occurrence	Brain Lobe
1	FT7-FT8	5	Frontal-Temporal	9	FP1-FP2	1	Frontal-Parietal
2	T9-T10	4	Temporal	10	AF3-AF4	1	Anterior-Frontal
3	F7-F8	3	Frontal	11	F1-F2	1	Frontal
4	T7-T8	3	Temporal	12	C3-C4	1	Central
5	F5-F6	2	Frontal	13	CP3-CP4	1	Central-Parietal
6	FC3-FC4	1	Frontal-Central	14	CP5-CP6	1	Central-Parietal
7	AF7-AF8	1	Anterior-Frontal	15	CP1-CP2	1	Central-Parietal
8	FC5-FC6	1	Frontal-Central	16	FC1-FC2	1	Frontal-Central

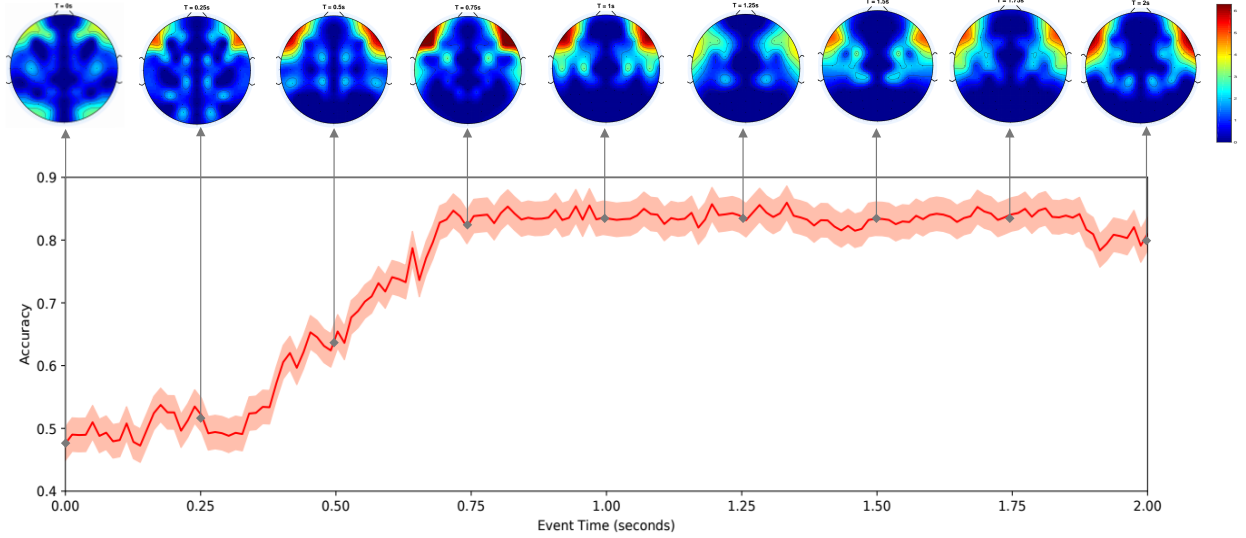


Fig. 6. Degree of each sensor usage in the top-30 subject-independent features

Moreover, at $t = 0.25s$ sensor pairs in the central-parietal (CP3-CP4 and CP5-CP6) lobes, as well as all the sensor pairs in the parietal lobe (P1-P2, P3-P4 and P5-P6) became more informative compared to $t = 0s$. This activity was also consistent with the phenomenon reported in previous studies, stating that the dorsal stream eventually reaches the parietal-cortex, which contains action-relevant information [56]. This is also supported by previous studies claiming that parietal lobe contributes predominantly to visual imagery and episodic memory [57].

At $t = 0.5s$, the active effect of sensor pairs in the parietal lobe diminished, which represents the completion of information flow in the dorsal stream. Consequently, sensor pairs in the central-parietal lobe (CP1-CP2, CP3-CP4 and CP5-CP6) became even more informative. This observed pattern was also consistent with previous related work claiming that parietal lobe also contributes to hand and upper limb control and eye movements with visual information [58].

At $t = 0.75s$, sensor pairs in temporal (T7-T8 and T9-T10), frontal (F7-F8) and anterior-frontal (AF7-AF8) lobes reached their highest degree of use, thus having the highest discriminability for L/R hand movements. This phenomenon was consistent with the fact explained by previous studies that the frontal lobe contains pre-motor cortex and primary

motor cortex (M1), where the pre-motor cortex first concatenates information from the parietal and frontal lobes, which is then delivered to M1. M1 is believed to be a generator of movement-specific commands [59]. Therefore, the classification rate reached its highest peak because of the completed information streams in occipital-temporal and occipital-parietal-frontal [56]. Then, due to the high usage of sensor pairs in M1, the classification rate remained unchanged until the movement ended [59].

Lastly, from $t = 0.75s$ to $t = 2.0s$, the sensor pairs in the temporal and frontal lobes maintained the highest degree of usage, while those in the parietal lobe were much less frequently used. The other sensor pairs in the occipital lobe barely contributed to the classification task.

VI. CONCLUSION

This paper proposed a novel solution for classification of L/R hand movements from EEG signals. First the negative effects of signal artifacts was reduced, improving the quality of data. In the next step, we exploited a wide range of time and frequency domain features, which were then used as an input to an attention-based LSTM network. After studying the optimal LSTM hyper-parameter settings, extensive experiments

were conducted with the EEG Motor Movement/Imagery Database over a large number of subjects (103). The performance evaluation with both intra-subject and cross-subject evaluation schemes showed very effective results with a high generalization capability, demonstrating the superiority of the proposed approach when compared to other benchmarking models and previous studies. The robust performance achieved in this paper suggests that the proposed method can be used in future research for a broad range of EEG-related classification tasks. Finally, a detailed analysis of the flow of EEG information through the sensors over time is presented, reflecting the brain activity throughout the experiment. Future work will focus on pushing the boundary on early classification upon perception of the stimuli, moving toward prediction instead of classification. Additionally, other deep learning techniques will be exploited to potentially further increase the accuracy.

ACKNOWLEDGMENT

The Titan XP GPU used for this research was donated by the NVIDIA Corporation.

REFERENCES

- [1] I. Käthner, S. C. Wriessnegger, G. R. Müller-Putz, A. Kübler, and S. Halder, "Effects of mental workload and fatigue on the p300, alpha and theta band power during operation of an erp (p300) brain-computer interface," *Biological Psychology*, vol. 102, pp. 118–129, 2014.
- [2] S. N. Abdulkader, A. Atia, and M.-S. M. Mostafa, "Brain computer interfacing: Applications and challenges," *Egyptian Informatics Journal*, vol. 16, no. 2, pp. 213–230, 2015.
- [3] J. J. Daly and J. R. Wolpaw, "Brain-computer interfaces in neurological rehabilitation," *The Lancet Neurology*, vol. 7, no. 11, pp. 1032–1043, 2008.
- [4] J. R. Wolpaw, N. Birbaumer, D. J. McFarland, G. Pfurtscheller, and T. M. Vaughan, "Brain-computer interfaces for communication and control," *Clinical neurophysiology*, vol. 113, no. 6, pp. 767–791, 2002.
- [5] M. Takahashi, K. Takeda, Y. Otaka, R. Osu, T. Hanakawa, M. Gouko, and K. Ito, "Event related desynchronization-modulated functional electrical stimulation system for stroke rehabilitation: a feasibility study," *Journal of neuroengineering and rehabilitation*, vol. 9, no. 1, p. 56, 2012.
- [6] L. R. Hochberg, M. D. Serruya, G. M. Fiehs, J. A. Mukand, M. Saleh, A. H. Caplan, A. Branner, R. D. Chen, R. D. Penn, and J. P. Donoghue, "Neuronal ensemble control of prosthetic devices by a human with tetraplegia," *Nature*, vol. 442, no. 7099, p. 164, 2006.
- [7] C. Guger, W. Harkam, C. Hertnaes, and G. Pfurtscheller, "Prosthetic control by an eeg-based brain-computer interface (bci)," in *Proc. aaate 5th european conference for the advancement of assistive technology*. Citeseer, 1999, pp. 3–6.
- [8] C. Guger, S. Daban, E. Sellers, C. Holzner, G. Krausz, R. Carabalona, F. Gramatica, and G. Edlinger, "How many people are able to control a p300-based brain-computer interface (bci)?" *Neuroscience letters*, vol. 462, no. 1, pp. 94–98, 2009.
- [9] E. A. Curran and M. J. Stokes, "Learning to control brain activity: A review of the production and control of eeg components for driving brain-computer interface (bci) systems," *Brain and cognition*, vol. 51, no. 3, pp. 326–336, 2003.
- [10] G. Pfurtscheller, C. Neuper, C. Guger, W. Harkam, H. Ramoser, A. Schlogl, B. Obermaier, and M. Pregenzer, "Current trends in graz brain-computer interface (bci) research," *IEEE transactions on rehabilitation engineering*, vol. 8, no. 2, pp. 216–219, 2000.
- [11] J. Cantillo-Negrete, J. Gutierrez-Martinez, R. I. Carino-Escobar, P. Carrillo-Mora, and D. Elias-Vinas, "An approach to improve the performance of subject-independent bcis-based on motor imagery allocating subjects by gender," *Biomedical engineering online*, vol. 13, no. 1, p. 158, 2014.
- [12] F. Lotte, C. Guan, and K. K. Ang, "Comparison of designs towards a subject-independent brain-computer interface based on motor imagery," in *2009 Annual International Conference of the IEEE Engineering in Medicine and Biology Society*. IEEE, 2009, pp. 4543–4546.
- [13] H. Wang and D. Xu, "Comprehensive common spatial patterns with temporal structure information of EEG data: minimizing nontask related EEG component," *IEEE Transactions on Biomedical Engineering*, vol. 59, no. 9, pp. 2496–2505, 2012.
- [14] O. D. Eva and A. M. Lazar, "Comparison of classifiers and statistical analysis for EEG signals used in brain computer interface motor task paradigm," *International Journal of Advanced Research in Artificial Intelligence*, vol. 4, no. 1, pp. 8–12, 2015.
- [15] R. Tomioka, K. Aihara, and K.-R. Müller, "Logistic regression for single trial EEG classification," in *Advances in Neural Information Processing Systems*, 2007, pp. 1377–1384.
- [16] S. Bhattacharyya, A. Khasnobish, A. Konar, D. Tibarewala, and A. K. Nagar, "Performance analysis of left/right hand movement classification from EEG signal by intelligent algorithms," in *IEEE Symposium on Computational Intelligence, Cognitive Algorithms, Mind, and Brain (CCMB)*, 2011, pp. 1–8.
- [17] Z. Tang, C. Li, and S. Sun, "Single-trial EEG classification of motor imagery using deep convolutional neural networks," *Optik-International Journal for Light and Electron Optics*, vol. 130, pp. 11–18, 2017.
- [18] Y. R. Tabar and U. Halici, "A novel deep learning approach for classification of eeg motor imagery signals," *Journal of neural engineering*, vol. 14, no. 1, p. 016003, 2016.
- [19] S. Hochreiter and J. Schmidhuber, "Long short-term memory," *Neural Computation*, vol. 9, no. 8, pp. 1735–1780, 1997.
- [20] K. M. Tsiouris, V. C. Pezoulas, M. Zervakis, S. Konitsiotis, D. D. Koutsouris, and D. I. Fotiadis, "A long short-term memory deep learning network for the prediction of epileptic seizures using EEG signals," *Computers in Biology and Medicine*, vol. 99, pp. 24–37, 2018.
- [21] D. Zhang, L. Yao, X. Zhang, S. Wang, W. Chen, and R. Boots, "Eeg-based intention recognition from spatio-temporal representations via cascade and parallel convolutional recurrent neural networks," *arXiv preprint arXiv:1708.06578*, 2017.
- [22] P. Wang, A. Jiang, X. Liu, J. Shang, and L. Zhang, "Lstm-based EEG classification in motor imagery tasks," *IEEE Transactions on Neural Systems and Rehabilitation Engineering*, vol. 26, no. 11, pp. 2086–2095, 2018.
- [23] P. Szczuko, "Rough set-based classification of EEG signals related to real and imagery motion," in *IEEE Signal Processing: Algorithms, Architectures, Arrangements, and Applications (SPA)*, 2016, pp. 34–39.
- [24] P. Szczuko, M. Lech, and A. Czyżewski, "Comparison of classification methods for EEG signals of real and imaginary motion," in *Advances in Feature Selection for Data and Pattern Recognition*. Springer, 2018, pp. 227–239.
- [25] P. Szczuko, "Real and imaginary motion classification based on rough set analysis of EEG signals for multimedia applications," *Multimedia Tools and Applications*, vol. 76, no. 24, pp. 25 697–25 711, 2017.
- [26] N. T. M. Huong, H. Q. Linh, and L. Q. Khai, "Classification of left/right hand movement EEG signals using event related potentials and advanced features," in *International Conference on the Development of Biomedical Engineering in Vietnam*. Springer, 2017, pp. 209–215.
- [27] A. Loboda, A. Margineanu, G. Rotariu, and A. M. Lazar, "Discrimination of EEG-based motor imagery tasks by means of a simple phase information method," *International Journal of Advanced Research in Artificial Intelligence*, vol. 3, no. 10, 2014.
- [28] Y.-P. Lin, C.-H. Wang, T.-P. Jung, T.-L. Wu, S.-K. Jeng, J.-R. Duann, and J.-H. Chen, "EEG-based emotion recognition in music listening," *IEEE Transactions on Biomedical Engineering*, vol. 57, no. 7, pp. 1798–1806, 2010.
- [29] M. H. Alomari, A. Samaha, and K. AlKamha, "Automated classification of l/r hand movement EEG signals using advanced feature extraction and machine learning," *arXiv preprint arXiv:1312.2877*, 2013.
- [30] I. Guyon and A. Elisseeff, "An introduction to variable and feature selection," *Journal of Machine Learning Research*, vol. 3, no. Mar, pp. 1157–1182, 2003.
- [31] L. Breiman, "Random forests," *Machine learning*, vol. 45, no. 1, pp. 5–32, 2001.
- [32] P. Zhou, W. Shi, J. Tian, Z. Qi, B. Li, H. Hao, and B. Xu, "Attention-based bidirectional long short-term memory networks for relation classification," in *Proceedings of Association for Computational Linguistics*, vol. 2, 2016, pp. 207–212.
- [33] Y. Wang, M. Huang, L. Zhao *et al.*, "Attention-based lstm for aspect-level sentiment classification," in *Proceedings of the 2016 conference on empirical methods in natural language processing*, 2016, pp. 606–615.
- [34] Z. C. Lipton, J. Berkowitz, and C. Elkan, "A critical review of recurrent neural networks for sequence learning," *arXiv preprint arXiv:1506.00019*, 2015.

- [35] S. Hochreiter, "The vanishing gradient problem during learning recurrent neural nets and problem solutions," *International Journal of Uncertainty, Fuzziness and Knowledge-Based Systems*, vol. 6, no. 02, pp. 107–116, 1998.
- [36] K. Greff, R. K. Srivastava, J. Koutník, B. R. Steunebrink, and J. Schmidhuber, "Lstm: A search space odyssey," *IEEE Transactions on Neural Networks and Learning Systems*, vol. 28, no. 10, pp. 2222–2232, 2017.
- [37] C.-C. Chiu, T. N. Sainath, Y. Wu, R. Prabhavalkar, P. Nguyen, Z. Chen, A. Kannan, R. J. Weiss, K. Rao, E. Gonina, N. Jaitly, B. Li, J. Chorowski, and M. Bacchiani, "State-of-the-art speech recognition with sequence-to-sequence models," in *IEEE International Conference on Acoustics, Speech and Signal Processing (ICASSP)*, 2018, pp. 4774–4778.
- [38] Z. Yang, D. Yang, C. Dyer, X. He, A. Smola, and E. Hovy, "Hierarchical attention networks for document classification," in *Proceedings of NAACL-HLT*, 2016, pp. 1480–1489.
- [39] J. Devlin, M.-W. Chang, K. Lee, and K. Toutanova, "Bert: Pre-training of deep bidirectional transformers for language understanding," *arXiv preprint arXiv:1810.04805*, 2018.
- [40] G. Schalk, D. J. McFarland, T. Hinterberger, N. Birbaumer, and J. R. Wolpaw, "Bci2000: a general-purpose brain-computer interface (BCI) system," *IEEE Transactions on Biomedical Engineering*, vol. 51, no. 6, pp. 1034–1043, 2004.
- [41] P. PhysioToolkit, "Physionet: components of a new research resource for complex physiologic signals," *Circulation*, v101 i23, e215-e220.
- [42] S. Merity, N. S. Keskar, and R. Socher, "Regularizing and optimizing lstm language models," *arXiv preprint arXiv:1708.02182*, 2017.
- [43] D. P. Kingma and J. Ba, "Adam: A method for stochastic optimization," *arXiv preprint arXiv:1412.6980*, 2014.
- [44] O. Aydemir and T. Kayikcioglu, "Decision tree structure based classification of eeg signals recorded during two dimensional cursor movement imagery," *Journal of neuroscience methods*, vol. 229, pp. 68–75, 2014.
- [45] M. Bentleimsan, E.-T. Zemouri, D. Bouchaffra, B. Yahya-Zoubir, and K. Ferroudji, "Random forest and filter bank common spatial patterns for eeg-based motor imagery classification," in *2014 5th International Conference on Intelligent Systems, Modelling and Simulation*. IEEE, 2014, pp. 235–238.
- [46] J. Deng, W. Dong, R. Socher, L.-J. Li, K. Li, and L. Fei-Fei, "Imagenet: A large-scale hierarchical image database," in *IEEE Conference on Computer Vision and Pattern Recognition (CVPR)*, 2009, pp. 248–255.
- [47] F. Lotte, A. Van Langenhove, F. Lamarche, T. Ernest, Y. Renard, B. Arnaldi, and A. Lécuyer, "Exploring large virtual environments by thoughts using a brain-computer interface based on motor imagery and high-level commands," *Presence: teleoperators and virtual environments*, vol. 19, no. 1, pp. 54–70, 2010.
- [48] L. Koessler, L. Maillard, A. Benhadid, J. P. Vignal, J. Felblinger, H. Vespignani, and M. Braun, "Automated cortical projection of eeg sensors: anatomical correlation via the international 10–10 system," *Neuroimage*, vol. 46, no. 1, pp. 64–72, 2009.
- [49] S. Zeki, J. Watson, C. Lueck, K. J. Friston, C. Kennard, and R. Frackowiak, "A direct demonstration of functional specialization in human visual cortex," *Journal of neuroscience*, vol. 11, no. 3, pp. 641–649, 1991.
- [50] A. D. Milner and M. A. Goodale, "Two visual systems re-viewed," *Neuropsychologia*, vol. 46, no. 3, pp. 774–785, 2008.
- [51] B. A. Wandell, S. O. Dumoulin, and A. A. Brewer, "Visual field maps in human cortex," *Neuron*, vol. 56, no. 2, pp. 366–383, 2007.
- [52] M. S. Worden, J. J. Foxe, N. Wang, and G. V. Simpson, "Anticipatory biasing of visuospatial attention indexed by retinotopically specific-band electroencephalography increases over occipital cortex," *Journal of Neuroscience*, vol. 20, no. RC63, pp. 1–6, 2000.
- [53] E. Donchin, K. M. Spencer, and R. Wijesinghe, "The mental prosthesis: assessing the speed of a p300-based brain-computer interface," *IEEE Transactions on Neural Systems and Rehabilitation Engineering*, vol. 8, no. 2, pp. 174–179, 2000.
- [54] S. Yang and F. Deravi, "On the usability of electroencephalographic signals for biometric recognition: A survey," *IEEE Transactions on Human-Machine Systems (HMS)*, vol. 47, no. 6, pp. 958–969, 2017.
- [55] D. L. Woods, J. M. Wyma, E. W. Yund, T. J. Herron, and B. Reed, "Factors influencing the latency of simple reaction time," *Human Neuroscience*, vol. 9, p. 131, 2015.
- [56] M. A. Goodale and A. D. Milner, "Separate visual pathways for perception and action," *Trends in Neurosciences*, vol. 15, no. 1, pp. 20–25, 1992.
- [57] T. Pflugshaupt, M. Nösberger, K. Gutbrod, K. P. Weber, M. Linnebank, and P. Brugger, "Bottom-up visual integration in the medial parietal lobe," *Cerebral Cortex*, vol. 26, no. 3, pp. 943–949, 2014.
- [58] L. Fogassi and G. Luppino, "Motor functions of the parietal lobe," *Current Opinion in Neurobiology*, vol. 15, no. 6, pp. 626–631, 2005.
- [59] R. P. Dum and P. L. Strick, "Motor areas in the frontal lobe of the primate," *Physiology & Behavior*, vol. 77, no. 4-5, pp. 677–682, 2002.